

Strong Bulk Photovoltaic Effect in Planar Barium Titanate Thin Films

Andrew L. Bennett-Jackson^{1,*}, Or Shafir^{2,*}, A. R. Will-Cole^{1,*}, Atanu Samanta², Dongfang Chen⁴, Adrian Podpirka¹, Aaron Burger³, Liyan Wu⁴, Eduardo Lupi Sosa⁵, Lane W. Martin^{5,6}, Jonathan E. Spanier^{1,3,4,7,†}, and Ilya Grinberg^{2,†}

¹*Department of Materials Science & Engineering,
Drexel University, Philadelphia, PA 19104-2875, USA*

²*Department of Chemistry, Bar-Ilan University, Ramat-Gan, Israel*

³*Department of Electrical & Computer Engineering,
Drexel University, Philadelphia, PA 19104-2875, USA*

⁴*Department of Mechanical Engineering & Mechanics,
Drexel University, Philadelphia, PA 19104-2875, USA*

⁵*Department of Materials Science & Engineering,
University of California at Berkeley, Berkeley, CA 94720, USA*

⁶*Materials Sciences Division, Lawrence Berkeley National Laboratory, Berkeley, CA 94720, USA and*

⁷*Department of Physics, Drexel University, Philadelphia, PA 19104-2875, USA*

The bulk photovoltaic effect (BPE) leads to the generation of a photocurrent from an asymmetric material. Despite drawing much attention due to its ability to generate photovoltages above the band gap (E_g), it is considered a weak effect due to the low generated photocurrents. Here, we show that a remarkably high photoresponse can be achieved by exploiting the BPE in simple planar BaTiO₃ (BTO) films, solely by tuning their fundamental ferroelectric properties via strain and growth orientation induced by epitaxial growth on different substrates. We find a non-monotonic dependence of the responsivity (R_{SC}) on the ferroelectric polarization (P) and obtain a remarkably high BPE coefficient (β) of $\approx 10^{-2}$ 1/V, which to the best of our knowledge is the highest reported to date for standard planar BTO thin films. We show that the standard first-principles-based descriptions of BPE in bulk materials cannot account for the photocurrent trends observed for our films and therefore propose a novel mechanism that elucidates the fundamental relationship between P and responsivity in ferroelectric thin films. Our results suggest that practical applications of ferroelectric photovoltaics in standard planar film geometries can be achieved through careful joint optimization of the bulk structure, light absorption, and electrode-absorber interface properties.

I. INTRODUCTION

The BPE in piezoelectric insulating crystals enables the generation of a photocurrent within the bulk interior of a solid and in principle, allows power conversion efficiencies (PCE) above the Shockley-Queisser (SQ) limit[1–6]. Since the excited carrier separation is carried out by the bulk of the material, the open-circuit voltage of a BPE-based device can be higher than the E_g , eliminating a major constraint on the PCE that leads to the SQ limit. Despite its promise to overcome this long-standing limit on the PCE of photovoltaic (PV) devices, BPE has been considered to be purely of academic interest for several decades following its discovery due to the high band gaps of typical ferroelectric (> 3.0 eV) and the very small photocurrents generated under illumination. The last decade has seen a resurgence of interest in BPE with advances in its theoretical understanding and in the design of BPE materials that have led to progress toward its use in practical devices [7–32]. Many new ferroelectrics with band gaps in the visible range have been developed, enabling greater absorption of light energy [33–39]. In theoretical studies, first-principles-based descriptions of shift-current and ballistic mechanisms of BPE have been

developed[15–17]. These showed that the BPE effect in a bulk material is weak, and the generated photocurrent is small for both mechanisms [17] (Table S1, Supporting Information). This is in agreement with the BPE currents observed in ceramic samples in the horizontal configuration where the sample is illuminated on the side and its top and bottom electrodes are separated by a larger (~ 1 mm) distance. However, experimental results on thin ferroelectric films in the vertical configuration, where the sample is illuminated through the top electrode and the bottom electrodes are separated by a small distance (10–500 nm) found much stronger photocurrents several orders of magnitude larger than those in bulk ceramic samples [40]. Furthermore, several studies have showed that even higher photocurrents can be obtained using nanoscale systems [13, 41, 42]. For example, above-the-SQ-limit PCE was obtained for BTO with nanoscale electrodes[7]. Similarly, a high β (equivalent to the R_{SC} , which is defined as the short-circuit current (J_{SC}) divided by the illumination power density) was obtained for strained MoS₂ and WS₂ nanotubes, with a $\beta \sim 1$ V⁻¹[40, 42]. This BPE coefficient value is orders of magnitudes higher than that for planar films and ceramics (Figure 1) [43]. These results suggest that while standard BPE may be unsuitable for practical use, high BPE photocurrent can be obtained through special nanoscale effects present in 1D and 2D nanoscale systems and in thin films with nanoscale electrodes. Nevertheless, the mechanism of these effects is

* A.L.B.-J., O.S. and A.R.W.-C. contributed equally to this work.

† email: spanier@drexel.edu, ilya.grinberg@biu.ac.il

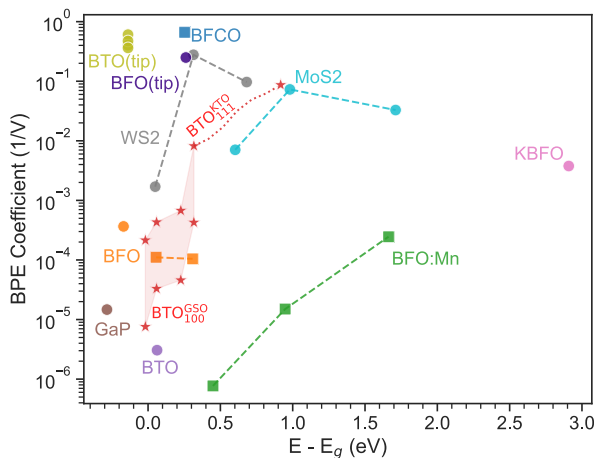


FIG. 1. Comparison of BPE coefficients for different materials as a function of incident energy above their corresponding E_g , adapted from Jiang et al.[42]. Bulk materials (MoS₂[42], WS₂ nanotubes[41], BTO[6] and tip-enhanced BTO (BTO(tip))[7], GaP[44, 45], BFO[46] and tip-enhanced BFO (BFO(tip))[12]) are presented in circles. Films (Bi₂FeCrO₆(BFCO)[11], KBiFeO₃(KBFO)[47], BFO[48] and Mn-doped BFO (BFO:Mn)[48]) are presented in squares. The BPE coefficients are the R_{SC} for all points, except for bulk BTO and bulk BFO which are the β_{31} and β_{22} , respectively. The BPE coefficients of all samples was measured in a vertical configuration, except for BFO:Mn, KBFO and WS₂ which were studied using a lateral configuration. The BPE coefficients measured for our BTO films are shown by stars marking the boundaries of the shaded region. Predicted responsivity of the BTO/KTO(111) film at illumination 1 eV above the gap according to its variations in the absorption coefficient is shown by stars connected by the dashed line.

currently unknown.

Several problems still hinder the further development and application of BPE materials. First, because the studies of BPE reported in the literature have been carried out on different absorbers and electrodes, it is difficult to extract trends and systematically analyze the BPE mechanisms and their dependence on material properties. The most basic example of this is the relationship between the degree of the structural asymmetry of the material as measured by its P or off-center B -site displacement (D) and the BPE photocurrent. While structural asymmetry of the absorber system is a fundamental requirement of BPE, its effect on the magnitude of the photocurrent is not currently understood. Phenomenological models of ballistic BPE [4, 49] suggest that the photocurrent has a polynomial scaling with the asymmetry, with the current density (J) proportional to either D^2 or D^3 , indicating that a strong enhancement of BPE can be obtained by increasing the material P (Section I and Section II, Supporting Information). By contrast, a theoretical study on (PbNiO₂)_x-(PbTiO₃)_{1-x} [50] and a joint experiment-theory study on La-doped BiFeO₃ (BFO)[24] that examined the effect of P variation on the

photocurrent found that smaller D and P lead to higher BPE response; however, this was ascribed to the E_g and enhanced light absorption in the less-polarized system, rather than to the effect of the asymmetry per se on the excited-carrier separation. Thus, the effect of asymmetry (or P) variation on BPE has not been elucidated to date and it is unclear whether and by how much BPE can be enhanced by increasing P . Even more importantly, the mechanisms of the effects that give rise to high BPE photocurrents that are much larger than those predicted by first-principles calculations and their interplay with the fundamental properties of the absorber material such as P have not been elucidated. Thus, the design principles for achieving a strong BPE-based response are currently unknown, with the exception of the need for the material to have a low E_g to ensure good light absorption which is general to all PV materials and is unrelated to BPE.

In this work, to understand the effect of the absorber P (or the asymmetry) on the BPE response in ferroelectric oxides, we study a series of planar BTO thin films grown on different substrates with the same planar electrodes. The different strain and orientation conditions of these films adjust the structural asymmetry of the BTO material, while leaving its chemistry and bonding largely unchanged. Thus, a comparison of the photocurrents obtained for these films will isolate the effect of the structural asymmetry on the BPE response. Our results for these BTO films show that the BPE photocurrent is governed by an interplay between the generation of asymmetric distributions of excited-carrier electrons that increases with increased cation displacement, and the collection of these carriers by the electrode that decreases exponentially with increasing cation displacement due to the effect of the Schottky barrier at the absorber-electrode interface [51]. We then show that a responsivity R_{SC} of 10^{-2} - 10^{-1} A/W can be obtained even for a standard planar indium tin oxide (ITO)/BTO/SrRuO₃ configuration, comparable to the R_{SC} or β achieved in recent nanoscale ferroelectric systems (Figure 1). Our results demonstrate that BPE is in fact a strong effect even when using standard planar electrodes, but its strength is often hidden by the effect of the poor excited carrier collection by the electrode due to the Schottky barriers at the absorber-electrode interface. This suggests that practical devices based on BPE may be possible and that creation of good absorber-electrode contacts should be emphasized in the further development of BPE-based devices. Furthermore, the contradiction between the weak BPE photocurrent predicted by the current theoretical models and the strong photocurrent observed in our work points out the need for further modeling efforts.

II. METHODOLOGY

BTO thin films (≈ 50 nm thick) were deposited by pulsed-laser deposition on (100)-oriented KTaO₃ (KTO) (two samples: KTO and KTO2), SrTiO₃ (STO), GdScO₃

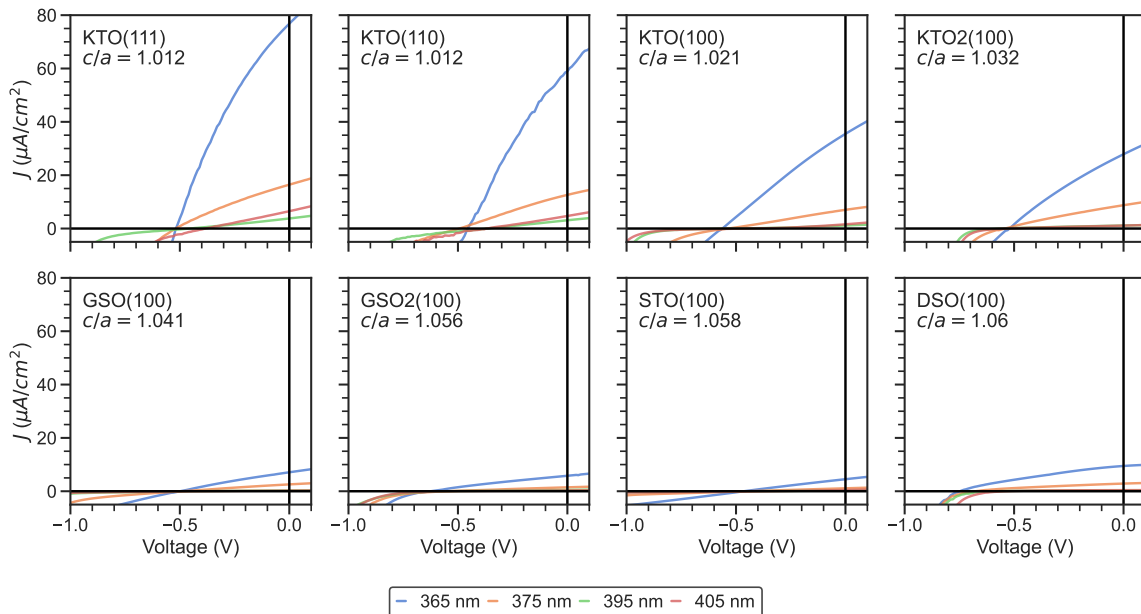


FIG. 2. Photovoltaic current-voltage traces for selected illumination wavelengths and BaTiO₃ film c/a ratios.

(GSO) (two samples: GSO and GSO2) and DyScO₃ (DSO) single-crystal substrates (MTI and CrysTech GmbH) following growth of a ≈ 15 nm-thick SrRuO₃ bottom-electrode layer (Section III, Supporting Information). In addition, BTO thin films were deposited on (110)- and (111)-oriented KTO substrates. Reciprocal space mapping (RSM) studies about the $(\bar{1}03)$, (222) , and (321) -diffraction conditions of the BTO and pseudocubic orthorhombic SrRuO₃ layers confirms that the deposited films are coherently strained with the GSO, DSO and KTO substrates and compressively strained, not unexpectedly, whereas that for the STO shows a purely horizontal shift and broadening compared with the bulk value[52], consistent with (partial) strain-relaxation and mosaicity of the film (Figure S1, Supporting Information). The c/a of each film was calculated from the RSM through a modified Bragg equation for a tetragonal unit cell (Table I and Section III, Supporting Information). The PV response of the films was studied under selected illumination wavelengths of 365, 375, 395 and 405 nm. The obtained V_{OC} , J_{SC} and R_{OC} are presented in I for 365 nm and in Table S2 in the Supporting Information for the other wavelengths. We use density functional theory (DFT) calculations to obtain the D , P and absorption coefficients (α) of BTO at the lattice parameters of the experimental films. The D , P and α under different c/a ratios calculations were carried out using five atoms BaTiO₃ unit cells. In each case, we impose the experimental lattice parameters of the studied film and performed the relaxation of the internal coordinates. All of the relaxations, Schottky barrier and bulk properties calculations were performed using the Quantum ESPRESSO package [53] with the Perdew-Burke-Ernzerhof (PBE) functional[54]. The optical properties were calculated using the ABINIT package[55]. In

all calculations, norm conserving pseudopotentials from the Pseudo-Dojo database were used[56]. The calculated D , P , E_g , and α at 365 nm are presented in Table I. The α at the other wavelengths can be found in Table S2 in the Supporting Information, alongside the absorption coefficient plot in Figure S2. For the parameters optimization and curve fitting, basin-hopping optimization was used as implemented in the SciPy package [57].

III. RESULTS

A. Experimental Results

Examination of the experimental J - V curves (Figure 2) of the (100)-oriented films shows several features characteristic of BPE, rather than the standard heterojunction effect (Section IV, Supporting Information). First, PV responses under selected illumination wavelengths show a linear J - V relationship at small V close to the short-circuit conditions and a rectifying-type J - V behavior only at large V (small J) close to the open-circuit conditions. The rectifying behavior is less prominent for the lowest wavelength of 365 nm and is largely the same for the other three wavelengths for all six (100)-oriented films. Second, we find that the open-circuit photovoltages (V_{OC}) at different intensities are essentially identical as expected for BPE and in contrast to the increased V_{OC} expected for increased light intensity for a heterojunction photocurrent generation mechanism. Third, we find that the photocurrent under linearly polarized illumination shows a sinusoidal variation with the rotation of the film that is expected for BPE (Figure S3 and Section IV, Supporting Information), indicating the presence of BPE

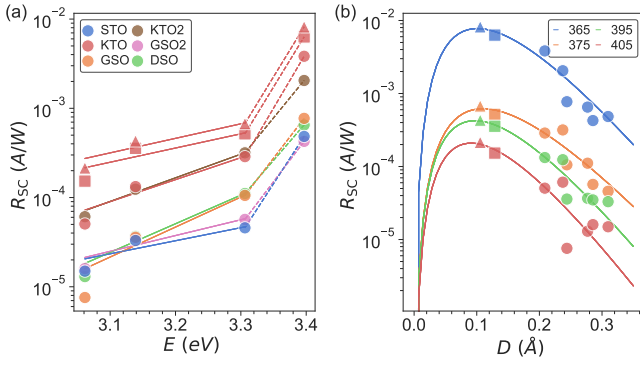


FIG. 3. Different scalings of the R_{SC} for the studied orientation samples. (a) R_{SC} variation as a function of incident energy. Exponential fit of the R_{SC} is plotted (solid lines) for each sample and is continued by an interpolation for the higher energy (dashed lines). (b) R_{SC} variation with the titanium displacement (D) of the sample in different incident wavelengths. Plotted lines are a fitting of the values for the function of $a_0 D^3 e^{-a_1 D}$ for 365 nm and $a_0 D^2 e^{-a_1 D}$ for the other wavelengths, fitted for all of the samples.

contribution. Finally, experiments using BTO doped on the B -site to become paraelectric at room temperature found a short-circuit current (J_{SC}) of essentially zero (Section V, Supporting Information), strongly suggesting that the photocurrent is generated due to the presence of asymmetry in the material that gives rise to BPE.

We then analyze the J_{SC} values extracted from the J - V curves. We first normalize J_{SC} by dividing by the illumination power density to obtain the R_{SC} and plot the obtained R_{SC} values versus the photon energy in a log-scale plot (Figure 3 (a)). It is observed that the R_{SC} data for the different BTO films show two different regimes, with a linear rise in R_{SC} on log-scale with photon energy observed for 405, 375 and 395 nm followed by a strong jump to much higher R_{SC} values at 365 nm. The decrease in BTO R_{SC} values from 365 nm to 405 nm is quite strong (factor of 40-100). Since the E_g of BTO is in the 3.1–3.3 eV range, we assign the difference in the response observed at 365 nm and the response at 375, 395 and 405 nm to the difference in the light absorption properties of BTO between these wavelengths, with the response at 365 nm due to interband transitions and the response observed at 375, 395 and 405 nm to the excitations from impurity states corresponding to the long tail in the BTO absorption spectrum.

Comparison of the R_{SC} data for the (100)-oriented films shows that for all wavelengths the R_{SC} decreases strongly (by a factor of more than 4) from the film grown on KTO to those grown on GSO, DSO and STO despite their higher c/a ratio, D and P (Figure 3(a), Table I and Table S2, Supporting Information). Meanwhile, R_{SC} is zero for the non-polar doped BTO sample (Section IV, Supporting Information). Comparison of the calculated E_g values for the different films shows only small E_g variations among the films (Table I). Thus, unlike in the

previous works [24, 50] that observed a similar trend of increasing R_{SC} with decreasing P , for our systems the changes in R_{SC} cannot be explained by the variation in the E_g . Additionally, as discussed above, a drastic drop in R_{SC} is observed experimentally from 365 nm to 375 nm for all films, indicating that for all films, the E_g is between these two wavelengths, in agreement with the DFT calculations. Comparison of the calculated α shows that the small changes in the E_g due to the changes in the c/a of the different films lead to only small changes in absorption that cannot account for the observed large variation in the experimental R_{SC} values with strain, c/a and P (Figure 3(a), Table I and Table S2, Supporting Information). For example, while the R_{SC} of the KTO(100)/BTO is almost an order of magnitude larger than that of GSO2(100)/BTO, the absorbance coefficient of GSO2(100)/BTO is $\sim 70\%$ of that of KTO(100)/BTO. Therefore, we conclude that the variation in the R_{SC} is due to the effect of the structural variations among the films as manifested by the changes in the c/a , titanium displacement D and polarization P of the films. Thus, the results for the (100)-oriented films show a non-monotonic dependence of R_{SC} on P .

Comparison of the R_{SC} values to the results in the literature shows that the R_{SC} values of our (100)-oriented films are higher than those for ceramics and are consistent with the R_{SC} values previously obtained for thin films in vertical configurations (Figure 1). The observed trend of increasing R_{SC} with decreasing P and D suggests that even higher R_{SC} values will be observed for smaller P and D values, with peak values reached between $D=0.0$ Å and $D=0.2$ Å.

To decrease the out-of-plane P and D further and examine the R_{SC} values in the $D=0.0-0.2$ Å range, we grew BTO films on KTO (110) and (111) substrates. As expected, we obtained much higher J_{SC} that corresponds to R_{SC} of 10^{-2} A/W, which is close to the values obtained for nanoscale systems, and is the largest value reported to date for BTO films (to the best of our knowledge). The non-monotonic dependence of R_{SC} on P suggests that the magnitude of the photoresponse is controlled by more than one effect. A log-scale plot of the R_{SC} values versus D (which determines P , Figure 3 (b)) reveals an exponential dependence of R_{SC} on D (and therefore on P) in the high- D region ($D > 0.2$ Å). Therefore, for simplicity, we empirically characterize the non-monotonic R_{SC} dependence on D as

$$R_{SC} = a_0 D^n e^{-a_1 D} \quad (1)$$

where a_0 and a_1 are constants and n is an integer. We fit the R_{SC} data to Equation 1 for $n = 1, 2$ and 3 (Figure S4, Supporting Information). We find that $n = 2$ and 3 give the best fit, with clearly poor matching between the fit and the experimental data obtained for $n = 1$. The fitting suggests that our BTO films grown on KTO (111) obtain close to the maximum possible R_{SC} values at 365 nm for BTO films. Similarly, good agreement is

TABLE I. Experimental lattice parameters, DFT-calculated D of titanium, P , E_g and α of each studied film, alongside their experimentally measured R_{SC} , V_{OC} , J_{SC} and fill factor (FF) at 365 nm. Rigid shift of 1.1 eV [58] is applied to the band gap to account for the underestimation of DFT.

| Substrate | c/a | a (Å) | c (Å) | E_g (eV) | D (Å) | P (Cm ⁻²) | α (10 ⁵ m ⁻¹) | R_{SC} (10 ⁻³ A/W) | V_{OC} (V) | J_{SC} (μA/cm ²) | FF |
|-----------|-------|------------|------------|---------------|------------|----------------------------|--|------------------------------------|-----------------|-----------------------------------|-------|
| KTO(111) | 1.012 | 3.990 | 4.036 | 3.083 | 0.106 | 0.187 | 4.810 | 8.190 | -0.519 | 77.247 | 0.293 |
| KTO(110) | 1.012 | 3.990 | 4.036 | 3.083 | 0.129 | 0.228 | 4.833 | 6.308 | -0.456 | 59.484 | 0.322 |
| KTO(100) | 1.021 | 3.989 | 4.074 | 3.078 | 0.209 | 0.367 | 4.008 | 3.830 | -0.567 | 35.732 | 0.271 |
| KTO2(100) | 1.032 | 3.989 | 4.116 | 3.071 | 0.237 | 0.413 | 3.449 | 2.050 | -0.515 | 24.100 | 0.290 |
| GSO(100) | 1.041 | 3.968 | 4.130 | 3.089 | 0.244 | 0.427 | 3.241 | 0.771 | -0.488 | 7.435 | 0.280 |
| GSO2(100) | 1.056 | 3.968 | 4.190 | 3.080 | 0.285 | 0.493 | 2.795 | 0.426 | -0.493 | 5.020 | 0.290 |
| STO(100) | 1.058 | 3.990 | 4.223 | 3.054 | 0.310 | 0.525 | 2.697 | 0.484 | -0.448 | 4.826 | 0.264 |
| DSO(100) | 1.060 | 3.945 | 4.182 | 3.102 | 0.277 | 0.485 | 2.773 | 0.651 | -0.747 | 7.670 | 0.313 |

obtained between the R_{SC} values for illumination at 375 and 395 nm and the $D^2 e^{-\alpha D}$ scaling of R_{SC} expected for the below-the-band-gap photon energies. For 405 nm, the fit is more poor, most likely due to the large relative error (scatter) of the R_{SC} values due to the small absolute magnitude of the response to illumination at 405 nm.

Our results demonstrate that a larger PV response can be obtained in standard planar BTO films by appropriately decreasing the polarization to $P \approx 0.18$ Cm⁻², which corresponds to a $D \approx 0.1$ Å. Furthermore, since BTO shows low absorption coefficient at 365 nm, a further increase in R_{SC} can be obtained by simply using a higher photon energy of light, reaching the R_{SC} magnitudes observed for the nanoscale systems. In fact, examination of R_{SC} of different ferroelectric systems reported in the literature plotted versus the difference between the photon energy and the E_g of the ferroelectric material in Figure 1 shows that our films achieve values comparable to those of the nanoscale WS₂ systems for the energy difference values. Thus, it is clear that even planar electrode BTO films can show strong photocurrent response that is much larger than that predicted by the first-principles calculations for the BPE photocurrent in BTO [16, 17].

B. Interpretation of the BTO film data in light of possible PV mechanisms

1. Possible BPE mechanisms underlying the observed short-circuit current data

To understand the observed variation in the BTO film R_{SC} values, we consider the possible mechanisms that can give rise to photocurrent in ferroelectric materials. Previous studies have explored several such mechanisms in the context of ferroelectric PV materials (Figure 4). In mechanism I, the excited charge carriers may be separated by the depolarizing field that can be quite strong in ferroelectric thin films. In mechanism II, the excited charge carriers may be separated by the standard heterojunction effect due to the presence of Schottky barriers at the fer-

roelectric absorber/electrode interfaces. In both of these mechanisms, the carriers are relaxed to the conduction band minimum and the carrier separation is due to the electric field present in the material (either due to the depolarization field or due to the electric field arising due to the Schottky barrier). Thus, these mechanisms are similar to those of the standard PV cells and are bound by the SQ limit. Alternatively, J_{SC} may be due to a hot-carrier effect.

In a hot-carrier PV mechanism (mechanism III), the photocurrent may be due to the unequal filtering of the excited hot carriers due to the difference between the Schottky barriers at the top and bottom interfaces. The unequal Schottky barriers may be due to either asymmetric electrodes or due to the effect of the polarization of the ferroelectric. In another hot-carrier mechanism that is specific to ferroelectric materials (mechanism IV), which was examined in previous studies [4, 16, 17], the photocurrent is due to the separation of the excited hot charge carriers due to the intrinsic asymmetry of the bulk material created by the spontaneous polarization, i.e., the BPE, either through the shift current or ballistic BPE current. For both of these hot-carrier mechanisms, the carriers are hot, the excited carrier separation is not due to the electric field in the material, and the cell efficiency is not bound by the SQ limit.

Consideration of our results shows that neither one of the standard PV mechanisms (Mechanisms I and II) can explain the experimental results. Since the depolarizing field (Mechanism I) is proportional to the surface charge of the material given by $P \cdot \vec{N}$, where \vec{N} is the surface vector, greater R_{SC} values should be obtained for systems with higher c/a (and therefore P/D), opposite from the decrease in R_{SC} from the KTO-grown sample (with lower c/a) to GSO-grown sample (with higher c/a) obtained for our BTO films. Similarly, for a heterojunction created by the Schottky barrier at the interface (Mechanism II) with a Schottky barrier height of Φ , the photocurrent is

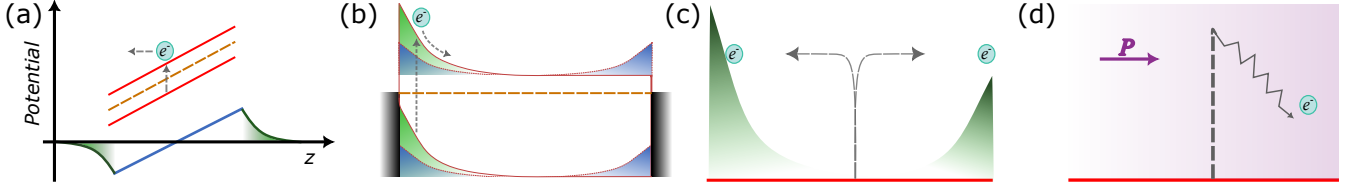


FIG. 4. Illustration of the described BPE mechanisms. (a) Mechanism I - macroscopic potential (blue) of a ferroelectric film (across the z -axis) with a depolarizing field (blue), giving rise to the spatial variation of the valence band, conduction band (red) and Fermi level (orange) and photocurrent due to the motion of the electrons at the conduction band minimum. (b) Mechanism II - band bending due to the formation of Schottky contact with the electrodes (black), showing the Schottky barriers with (green) and in the absence (blue) of ferroelectric polarization. The excited carriers are affected by the field at the Schottky barrier, giving rise to the photocurrent due to the motion of the electrons at the conduction band minimum. (c) Mechanism III - hot carrier electrons are generated and then are asymmetrically scattered from and transmitted through the Schottky barriers at the two ferroelectric-electrode interfaces. (d) Mechanism IV - Asymmetric momentum distribution of hot electrons in the direction of polarization due to the ballistic current BPE.

given by [13, 49]

$$\ln(I) = \left[\ln(AA^*T^2) - \frac{q\Phi^0}{k_B T} \right] + \frac{q\Phi}{k_B T} \left(\frac{q^3 N_{\text{eff}}}{8\pi^2 \epsilon_0^3 \epsilon_{\text{op}}^2 \epsilon} \right)^{1/4} (V + V_{bi}') \quad (2)$$

where A is the electrode area, A^* is the Richardson constant, T is the temperature, k_B is the Boltzmann constant, Φ^0 is the Schottky barrier height without the effect polarization, N_{eff} is the effective charge concentration, ϵ_0 is the vacuum permittivity, ϵ is the dielectric constant of the heterostructure, ϵ_{op} is the optical dielectric constant, V is the voltage, V_{bi} is the built-in voltage and V_{bi}' is the total potential incorporating the effects of ferroelectric polarization. V_{bi} and V_{bi}' are given by

$$\begin{aligned} V_{bi} &= \Phi^0 - \frac{k_B T}{q} \ln(N_c/n_e) \\ V_{bi}' &= V_{bi} + \frac{P}{\epsilon_0 \epsilon} \delta \end{aligned} \quad (3)$$

where N_c is the effective density of states in the conduction band, δ is the distance between the polarization charge sheet and the BTO/electrode interface, and n_e is the concentration of free electrons.

For our set of BTO films with different P , the only parameters in the heterojunction model that will vary among the films are ϵ and V_{bi}' because these parameters depend on P . A greater P due to the strain imposed by the substrate gives higher V_{bi}' and lower ϵ . A higher V_{bi}' in turn should result in a higher photocurrent (due to the greater field in the Schottky barrier region that gives rise to better carrier separation). Therefore, according to the heterojunction model, R_{SC} is expected to increase with increasing P in disagreement with the non-monotonic trend for R_{SC} as a function of P observed for our films. Furthermore, for both the depolarizing field and Schottky barrier heterojunction mechanisms, the V_{OC} should show

some dependence on the illumination intensity. However, as shown in the J - V curves (Figure 2), no such dependence is observed and the same V_{OC} values are obtained for all light powers. Thus, we conclude that these standard PV mechanisms cannot explain our results, and we therefore consider the hot-carrier mechanisms (mechanisms III and IV).

Mechanism III (filtering of hot carrier by the uneven Schottky barriers at the top and bottom interfaces) can in principle obtain the non-monotonic dependence of R_{SC} on P observed in our films. For the non-polar material, if the Schottky barriers at both electrode interfaces are either the same or close enough such that the excited hot carriers moving up and down are filtered equally by the Schottky barriers at the two interfaces, negligible or zero photocurrent will be observed. Since the height of the Schottky barrier is known to increase with greater P [39, 59] in ferroelectrics such as BTO and create differences between the Schottky barrier heights of the top and bottom interfaces, an increase in P will lead to greater filtering of hot-carriers by one interface compared to the other, so that a non-negligible R_{SC} will be obtained. The photocurrent will initially increase with increasing P due to the greater difference between the two Schottky barrier heights. Then, as the Schottky barrier height becomes large, too many hot carriers will be filtered out and the R_{SC} will decrease, so that a non-monotonic dependence of R_{SC} on P will be observed. However, numerical modeling of this mechanism (see SI) could not reproduce the observed $a_0 D^n e^{-a_1 D}$ ($n = 2, 3$) dependence of R_{SC} , even when we considered the dependences of the Schottky barrier height on D at the top and bottom interfaces as different adjustable parameters in the model.

Considering mechanism IV, we find that the observed variation of R_{SC} with c/a and P/D also cannot be explained based on the shift and ballistic current mechanisms of BPE in bulk BTO explored in first-principles calculations. For shift current, previous calculations showed that the variation in the current at the energy slightly above the E_g between different phases of BTO is $\sim 20\%$

[17] and similar for PbTiO_3 [16] around the gap. These variations are much smaller than a factor of 5 change in R_{SC} between the low c/a KTO-grown BTO film and high c/a GSO-grown BTO film. Additionally, the magnitudes of J_{SC} found for our BTO films grown on KTO(110) and KTO(111) substrates are several orders of magnitude higher than the J_{SC} values predicted by first-principles calculations for bulk BTO under illumination at 365 nm [17].

Additionally, the non-monotonic dependence of J_{SC} on P of our film is inconsistent with the increase in the photocurrent with increasing P expected for the ballistic current. According to the phenomenological theory of the ballistic BPE, the short-circuit current is given by

$$J_{\text{SC}} = ql_0\xi\phi\alpha\varphi_{\text{opt}} \quad (4)$$

where q is the electron charge, l_0 is the thermalization length, ξ is a parameter characterizing the asymmetry of the current generated by the excitation, ϕ is the quantum yield and φ_{opt} is the photon flux. As explained above, the small change in E_g between the low c/a (and low P) KTO-grown sample and the high c/a (and high P) GSO-grown sample mean that the changes in the contributions of α and l_0 between these two systems are small, while q , ϕ and φ_{opt} are either identical for all of our films or are also expected to vary slightly. Thus, a strong variation in the J_{SC} and R_{SC} values can only arise from the changes in the ξ parameter.

According to the previously developed phenomenological theory of ballistic photocurrent arising from band-to-band transitions and hot-carrier scattering from phonons, the asymmetry expressed by ξ in Equation 4 is proportional to the asymmetric transition probability $W_{k',k}$, *i.e.*, the imaginary part of the probability of scattering of an electron from momentum k to k' (Section I, Supporting Information):

$$W_{k',k} = c_1^2 \frac{2m}{\hbar} \int \frac{d^3k''}{(2\pi)^3} V_{k,k'} V_{k',k''} V_{k'',k} \frac{1}{\epsilon - \epsilon_{k''} + i\eta} \quad (5)$$

where $c_1 = -\frac{m}{2\pi\hbar}$, $V_{k,k'} = \langle k|V|k'\rangle$, $V_{k',k''} = \langle k'|V|k''\rangle$ and $V_{k'',k} = \langle k''|V|k\rangle$. The kets $|k\rangle$, $|k'\rangle$, and $|k''\rangle$ are the Bloch states of the system, and $\epsilon_{k''}$, $\epsilon_{k'}$ and ϵ_k are their corresponding eigenvalues. The scattering potential, V , is the asymmetric part of the potential generated by ionic displacement from the high-symmetry state. Expanding V in a Taylor series around the high-symmetry structure as a function of the ionic displacement D , the magnitude of V is given by $V(D) = (dV/dD)D + 1/6(d^2V/dD^2)D^2 + \dots$. Taking only the lowest-order term in this expansion, we obtain that ξ should be proportional to D^3 , and therefore, $J_{\text{SC}} \propto \alpha l_0 D^3$. A similar argument can be made for the ballistic current due to scattering/excitation by impurities (Section II, Supporting Information), except that in this case, the photocurrent is expected to be proportional to $\alpha l_0 D^2$. The expected scaling of R_{SC} with D^3 or D^2 is obviously inconsistent with the experimental results for

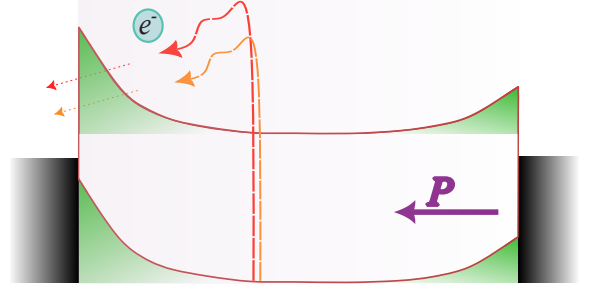


FIG. 5. Illustration of the proposed BPE mechanisms. Asymmetric momentum distribution of hot electrons in the direction of polarization is generated by BPEE. The non-thermalized electrons travel ballistically toward the interface and then only a fraction of these electrons is transmitted through the Schottky barrier.

our BTO films, indicating that the non-monotonic trend of R_{SC} with D cannot be explained even phenomenologically by the ballistic current mechanism of BPE in Equation 4.

Since the obtained R_{SC} values cannot be explained by the model of the BPE focusing solely on the absorber that is represented in Equation 4, we attribute the non-monotonic variation of R_{SC} with P to the combination of the effect of the asymmetry of the film leading to BPE and the effect of the Schottky barriers at the absorber-electrode interfaces. The photocurrent described by Equation 4 assumes a mechanism in which the excited electrons are sufficiently energetic to be transported over the Schottky barrier at the absorber-electrode interface [49]. This assumption is not necessarily reasonable for the interband transitions generated by 365 nm (3.4 eV) illumination with energy that is only slightly larger than the E_g . For such illumination, the changes in Φ will have a strong effect on the photocurrent collected by the electrode due to the exponential dependence of the photocurrent on the changes in the excited electron energy. For a ferroelectric-electrode interface, the Φ increases with increasing P [13, 59, 60], so that higher Schottky barriers and lower photocurrent can be expected for BTO films with higher c/a , P and D . On the other hand, for a non-polar material, there is no BPE so that no photocurrent is generated. Therefore, we assign the observed decrease in the photocurrent for films with greater P to the higher Schottky barriers of the more strongly polar films, with the observed photocurrent described by a modification of Equation 4 as

$$J_{\text{SC}} = e^{-\kappa\Phi} ql_0\xi\phi\alpha\varphi_{\text{opt}} \quad (6)$$

where κ is an empirical parameter and Φ is linearly proportional to the out-of-plane P (an ionic displacement) of the BTO film.

Phenomenologically, to first order, ξ should be proportional to D for any BPE mechanism, while for the ballistic current generated by the phonon mechanism, as described above ξ is proportional to D^3 and for the impurity mechanisms it is proportional to D^2 . Therefore, according to Equation 6, for 365 nm illumination, J_{SC} can

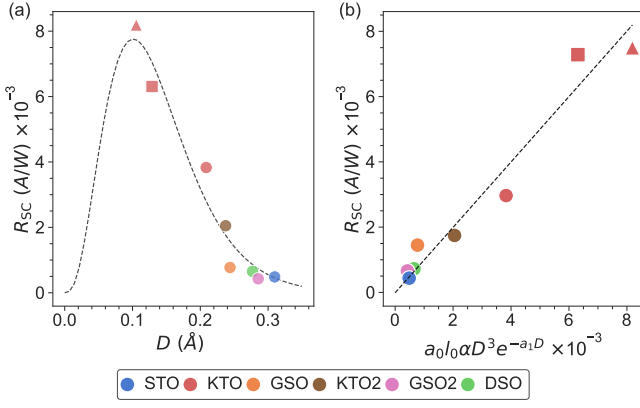


FIG. 6. (a) Variation of the R_{SC} at 365 nm illumination as a function of D for the different samples in the (100), (110) and (111) orientations (circles, square and triangle, respectively), alongside a fitting of R and $a_0 l_0 \alpha D^3 e^{-a_1 D}$ (dashed line). (b) R_{SC} at 365 nm illumination as a function of the predicted R_{SC} using $a_0 l_0 \alpha D^3 e^{-a_1 D}$.

be expected to scale as $D^n e^{-\kappa\Phi}$ where $n = 1 - 3$, matching the empirically fitted non-monotonic dependence of R_{SC} on D (Figure 3(a)). For excitation at below-the-gap photon energies, the asymmetry parameter ξ of the ballistic current mechanism should scale as D^2 (section VI, Supporting Information), so that J_{SC} will scale as $D^n e^{-\kappa\Phi}$ where $n = 1 - 2$. Thus, R_{SC} will first increase and then decrease with increasing D , matching the experimentally observed trend in the R_{SC} values (Figure 3 (a)). As shown in Figure S2 (Supporting Information), using the DFT calculated values for the absorption coefficient α and assuming that ξ is proportional to either D^2 or D^3 we obtain excellent fits to Equation 6 for the experimentally obtained R_{SC} under illumination at 365 nm (Figure 6) and the other illumination wavelengths (Figure S5 and Figure S6). Thus, the proposed mechanism is consistent with our R_{SC} data.

2. Modeling of the experimental J - V plots

The consideration of the effect of the Schottky barrier can also explain the non-linear J - V plots and their variation of these plots between the different BTO systems studied in our work. In the classic theory of BPE, the current at an applied bias potential V is given by

$$J(V) = J_{BPE} - J_{opposite} \quad (7)$$

where J_{BPE} is the BPE current and $J_{opposite}$ is the current induced by the applied bias voltage that arises from the electric field experienced by the excited hot carriers in the presence of the applied bias such that

$$J_{opposite} = (\sigma_{ph} + \sigma_{dark})V/d \quad (8)$$

where σ is the conductivity and is given as the sum of the conductivity contributions by the excited carriers σ_{ph} and the conductivity in the dark σ_{dark} , V is the applied bias and d is the thickness of the absorber. It is easy to see that this will give a linear dependence of J on V . Since $\sigma_{ph} \gg \sigma_{dark}$, the observed current will be given by

$$J(V) = ql_0 \xi \phi \alpha \varphi_{opt} - \sigma_{ph} V/d, \quad (9)$$

and the open-circuit voltage will be given by

$$V_{OC} = J_{SC} d / \sigma_{ph}. \quad (10)$$

Since σ_{ph} is proportional to the number of excited carriers which is proportional to ϕ , φ_{opt} and α , the V_{oc} will be independent of light illumination intensity.

While such linear dependence has always been observed for bulk BPE systems, the recently studied films in some cases show fairly nonlinear dependence of J on V [13], while in other cases bulk-like linear or almost linear dependence of J on V has been observed [13, 14]. For our films, the GSO-grown film has a close to linear J - V dependence, while as the P values decrease and the J_{SC} increases, the J - V dependence becomes more non-linear (Figure 2). However, in all cases, the V_{OC} is independent of the light intensity. We suggest that the observed variation in J - V curvature is due to the Schottky barrier effect. If the effects of Schottky barriers at the top and bottom of the film are taken into account, the expression for $J(V)$ should be modified to

$$J(V) = ql_0 \xi \phi \alpha \varphi_{opt} e^{-\kappa_t \Phi_t} - V/d \sigma_{ph} e^{-\kappa_b \Phi_b} \quad (11)$$

where t and b denote the top and bottom electrode, respectively. In this case, only some fraction of the excited hot carriers traveling toward the top interface (comprising J_{BPE}) and the bottom interface (comprising $J_{opposite}$) are actually extracted into the electrode. Furthermore, the polarization of a thin film will be affected by the applied bias field and this in turn will affect the Schottky barrier height. The dependence of P on V is given by

$$P = P_0 - \epsilon V/d \quad (12)$$

where d is the thickness of the film. Assuming a linear dependence of Φ on P , the Φ are given by

$$\begin{aligned} \Phi_t &= \Phi_t^0 - \gamma_t P \\ \Phi_b &= \Phi_b^0 - \gamma_b P \end{aligned} \quad (13)$$

where γ_t and γ_b are constants. Thus, an applied bias that decreases P will lead to smaller Φ at both the top and bottom interfaces. Additionally, due to the proportionality between P and ξ , an applied bias that decreases P will, in turn, decrease ξ . It can be shown that Equation 11 predicts that more strongly non-linear J - V curves will be obtained for films with smaller polarization, greater

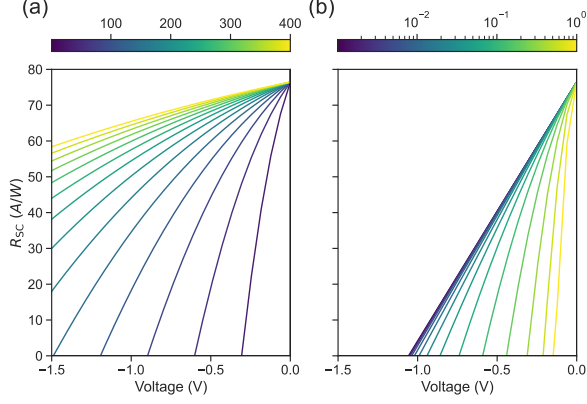


FIG. 7. The effects of (a) d and (b) ϵ on the J - V curves due to the proposed mechanism. The J - V curves are obtained using Equation 11. For (a) all parameters are fixed except for d and for (b) all parameters are fixed except for ϵ . As the d increases, the P of the film is less sensitive to the applied bias and tends toward a linear J - V relationship. The same effect is observed for decreasing ϵ that is usually found in films with larger P values.

sensitivity of polarization to electric field, and lower thickness. By contrast, very thick films and strongly polar films will show a lower J - V curvature (Figure 7). This is in agreement with the results obtained for our films. The strongly polar GSO-grown film with high D , P and c/a show almost linear dependence of J_{sc} on V , while the curvature of the J - V dependence increases strongly as the out-of-plane D and P decrease. We fit the J - V curves (Figure 2) obtained for our films to Equation 11 and find that a good match with the experimental data is obtained (Figure 8 using the fitting parameters specified in Table S3 in the Supporting Information). Thus, Equation 11 accurately describes the J - V curves of our BTO films.

It is important to point out here that in contrast to the standard PV materials, a higher FF value is actually unfavorable for the ferroelectric systems that follow the BPE-Schottky barrier mechanism. In the absence of the Schottky barrier effect, a linear J - V relationship would be obtained, whereas due to the Schottky barrier effect, the $J(V)$ decreases more rapidly (Figure 7) and a lower V_{oc} is obtained. However, due to the non-linearity of the J - V relationship, such a curve will exhibit a higher FF. Nevertheless, it is clear that the extracted power density is larger for the linear J - V relationship with a FF of 0.25 than for the non-linearity of the J - V relationship with FF larger than 0.25 (Table S2, Supporting Information).

C. Interpretation of previous results for ferroelectric PV

An examination of the results reported in a previous study by Tan et al.[13] suggests that they can be explained by the proposed mechanism (Mechanism V) of the joint effects of BPE and Schottky barriers expressed by Equation 11. Tan et al.[13] studied the dependence of J_{sc} , V_{oc} and the PCE on the film thickness in ultra-thin $\text{Pb}(\text{Zr}_{0.2}\text{Ti}_{0.8})\text{O}_3$ (PZT) films. They found that J_{sc} and PCE increased with lower film thickness, reaching high values of $\sim 2 \text{ mA/cm}^2$ and 2.49%, respectively, for a 12-nm-thick film. Interestingly, the V_{oc} did not show a strong increase for lower film thickness and increasingly non-linear J - V curves were observed as the film thickness changed from 300 nm (almost linear) to 120 nm (very curved). Tan et al.[13] ascribed their results to a heterojunction effect described by Equation 2. However, the obtained J - V curves can be also fit well by Equation 11 as can be seen in Figure 8 (b) and (c) (fitting parameters are presented in Table S4 and Table S5, Supporting Information), showing that their results are consistent with the BPE-Schottky barrier mechanism that predicts stronger J - V non-linearity for thinner film. Several other reports of thin-film ferroelectric PV in the literature show a trend of increasing J - V non-linearity with thinner films[61–63]. While in several cases, these effects were ascribed to heterojunction, in light of our results for the BTO films here, it is likely that in fact they are also due to the BPE-Schottky barrier mechanism.

As discussed above, recent studies of 1D and 2D systems found larger J_{sc} , R_{sc} and PCE values that were ascribed to BPE. Similarly, extremely high J_{sc} values and R_{sc} values were obtained by Spanier et al. [7] for BTO with nanostructured electrodes. In these studies the J - V relationship was linear. As discussed above, this suggests that the low gap (for the 1D and 2D systems) and the strong band bending due to nanostructured electrodes (for BTO of Spanier et al.[7]) eliminates the Schottky barrier in these systems, obtaining an Ohmic contact and the corresponding high PV response. Thus, it is likely that the high performance of these system is at least in part not due to a nanoscale electrode effect per se but rather simply due to the creation of favorable Ohmic contact that allows the full collection of excited hot carriers.

D. Possible origin of the strong BPE in planar films

We now discuss the origin of the high BPE R_{sc} that is much higher (even in the presence of the Schottky barrier effect) than the values predicted by first-principles calculations. In a bulk ferroelectric material, ballistic photocurrent arises either from the scattering of the hot carriers from asymmetric impurities or from phonons, both of which generate a asymmetric potential that affects the Bloch states of the system. However, as shown

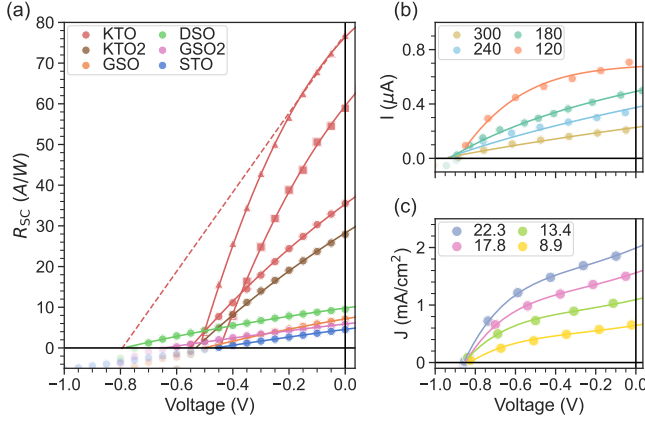


FIG. 8. (a) R_{SC} - V experimental data for illumination at 365 nm for our BTO films (symbols) with fits of R_{SC} to the suggested model equation (solid lines), alongside an extrapolation of the initial linear response at low voltages for the KTO(111) sample. Fitting was done for the positive R_{SC} range. (b) I - V curves of PZT films with different thicknesses (Å) studied by Tan et al.[13] together with fits to the suggested model (solid lines). (c) J - V curves of PZT films under different illumination intensity (mW/cm^2) studied by Tan et al.[13] together with fits to the suggested model (solid lines).

by first-principles calculations [17], both of these effects are weak. Nonetheless, in a thin ferroelectric film an additional source of asymmetric scattering is present, namely the deviation of the film structure from periodicity near the ferroelectric-electrode interface. While ferroelectric-electrode systems are often idealized as a simple combination of ferroelectric and electrode, in practice the presence of the electrode affects the structure of the ferroelectric film in the vicinity of the interface, generating deviation from the bulk structure. For example, band bending and a curved electrostatic potential in the vicinity of the interface (Figure 4) will lead to an aperiodic structure close to the electrode, in contrast to the periodic structure obtained in the presence of a linearly changing V arising from the presence of the depolarizing field. Such deviation from periodicity will act as an impurity and give rise to a ballistic photocurrent for the electrons excited in the vicinity of the ferroelectric-electrode interface. In contrast to impurities that typically have a very low concentration, the deviation from the bulk periodic structure occurs in every unit cell of the top layers of the ferroelectric films. Thus, the asymmetric scattering that gives rise to ballistic photocurrent should be much stronger in the thin film in the vicinity of the electrode than that arising from the presence of impurities in the bulk system. We suggest that this impurity-like scattering is the origin of the extremely high R_{SC} values observed in our films and in other recent experiments on ferroelectric BPE devices. This hypothesis suggests that engineering of greater deviation from periodicity either through the modification of the ferroelectric-electrode interface or by targeted growth of

impurity layers can be used to further increase the R_{SC} and PCE of ferroelectric PV devices.

IV. CONCLUSION

Our results show that the electrode-absorber interface, the orientation of the out-of-plane P relative to the crystal axis and the local structure must be taken into account in the design of BPE-based devices. Simple changes of the film orientation and strain conditions can result in up to a factor of 33 difference in the R_{SC} and the generated photocurrent. Specifically, for the BTO film grown on KTO(111) substrate, R_{SC} reaches $\approx 10^{-2}$ A/W in a planar-electroded device due to the weaker Φ effect that allows collection of a greater fraction of the generated bulk photocurrent. Considering the weak absorption of BTO at 365 nm, R_{SC} can be increased to 10^{-1} simply by enhancing absorption using higher photon energies. Such high values of R_{SC} are comparable to those obtained for devices based on ferroelectric WS_2 and MoS_2 nanotubes and for devices based on the tip enhancement effect (Figure 1).

This suggests that the high responsivities observed in these nanoengineered systems may not be due to a nanoscale electrode effect per se or to the changes to the bulk carrier separation mechanism, but rather to the reduction of the Schottky barrier. The good fit of the experimental data obtained for our BTO films to Equation 11 suggests that even for the BTO film grown on $\text{KTO}_3(111)$, a Schottky barrier still exists and prevents some fraction of excited carriers from being collected by the electrodes. This suggests that a realization of an Ohmic contact should enable an even higher R_{SC} , perhaps reaching as high as 1 A/W. Thus, our results demonstrate that BPE is in fact a strong effect for thin-film systems that is often masked by the weak light absorption due to the large gap of the absorber and by the poor carrier collection due to the Schottky barrier at the absorber-electrode interface.

Consideration of our results suggests the following research directions for achieving high R_{SC} and PCE in ferroelectric PV thin-film devices. First, it is vital to increase the amount of the light absorbed by the film. As shown in Table S2, the absorption coefficient at the energies just above the gap usually used to probe ferroelectric PV is relatively low. Our experimental results show that an increase in the photon energy to up to 1 eV above the gap will lead to a dramatic increase in R_{SC} (Figure 1). Thus, it is necessary to increase the light absorption of the film by decreasing the E_g while ensuring that the absorption mechanism allows a high value of α (i.e. the across-the-gap transition should not be dipole-forbidden). Second, it is necessary to eliminate the deleterious effect of the Schottky barrier. As shown by Cao et al[14], a 1-2 orders of magnitude increase in the photocurrent can be obtained by creating an Ohmic contact between the ferroelectric absorber and the electrode. Similarly, our

result for illumination at higher photon energies (Figure 2) show that R_{SC} is significantly increased by the improved collection of excited hot carriers with higher energies due to their better transmission through the Schottky barrier. Finally, to obtain a high V_{OC} , the P of the film should be stable in the presence of the applied V , allowing the favorable linear J - V relationship to be obtained. This suggests that ideally, highly polar materials such as PZT should be used. For theoretical research, further efforts are necessary to develop a microscopic, first-principles-based description of the strong BPE effect in thin films that incorporates the effect of the interface and enables first-principles calculations to provide guidance for further BPE device design efforts.

ACKNOWLEDGMENTS

The authors thank V. Fridkin, R. Agarwal and M.W. Cole for discussions. This work was supported at Bar-Ilan University and Drexel University by the NSF-BSF under grant no. CBET 1705440. The authors also acknowledge support at Bar-Ilan, Drexel and the University of California at Berkeley from the ARO under grant no. W911NF-21-1-0126 and from the NSF at Drexel under grant no. DMR 1608887 and UC Berkeley under grant no. DMR 2102895. A.L.B.-J. acknowledges support from the National Workforce Diversity Pipeline program of the Dept. of HHS under grant. no. CPIMP151091. D.C. and L.W.M. acknowledge support from the Army/ARL under Collaborative for Hierarchical Agile and Responsive Materials (CHARM) under cooperative agreement W911NF-19-2-0119, and from the Director's Innovation Initiative under 21-C-0090. The authors also acknowledge the Singh Center for Nanotechnology by the NSF Nanotechnology Coordinated Infrastructure Program under grant no. NNCI-1542153, the Drexel University Materials Characterization Facility (NSF DMR 1040166) and K. Chen, X. Xi and the Temple University College of Science and Technologies Research Facilities.

-
- [1] A. Grekov, M. MA, V. Spitsyna, and V. Fridkin, Soviet physics crystallography, USSR **15**, 423 (1970).
 - [2] A. Glass, D. von der Linde, and T. Negran, Applied Physics Letters **25**, 233 (1974).
 - [3] W. Koch, R. Munser, W. Ruppel, and P. Würfel, Solid State Communications **17**, 847 (1975).
 - [4] V. Belinicher and B. I. Sturman, Soviet Physics Uspekhi **23**, 199 (1980).
 - [5] V. M. Fridkin, *Photoferroelectrics*, Vol. 9 (Springer Science & Business Media, 2012).
 - [6] B. I. Sturman and V. M. Fridkin, *Photovoltaic and photo-refractive effects in noncentrosymmetric materials* (Routledge, 2021).
 - [7] J. E. Spanier, V. M. Fridkin, A. M. Rappe, A. R. Akbashahev, A. Polemi, Y. Qi, Z. Gu, S. M. Young, C. J. Hawley, D. Imbrenda, *et al.*, Nature Photonics **10**, 611 (2016).
 - [8] A. P. Kirk and D. W. Cardwell, Nature Photonics **11**, 329 (2017).
 - [9] J. E. Spanier, V. M. Fridkin, A. M. Rappe, A. R. Akbashahev, A. Polemi, Y. Qi, Z. Gu, S. M. Young, C. J. Hawley, D. Imbrenda, *et al.*, Nature Photonics **11**, 330 (2017).
 - [10] R. Nechache, C. Harnagea, S. Li, L. Cardenas, W. Huang, J. Chakrabartty, and F. Rosei, Nature photonics **9**, 61 (2015).
 - [11] R. Nechache, C. Harnagea, S. Licoccia, E. Traversa, A. Ruediger, A. Pignolet, and F. Rosei, Applied Physics Letters **98**, 10.1063/1.3590270 (2011).
 - [12] M. Alexe and D. Hesse, Nature communications **2**, 1 (2011).
 - [13] Z. Tan, L. Hong, Z. Fan, J. Tian, L. Zhang, Y. Jiang, Z. Hou, D. Chen, M. Qin, M. Zeng, *et al.*, NPG Asia Materials **11**, 1 (2019).
 - [14] D. Cao, C. Wang, F. Zheng, W. Dong, L. Fang, and M. Shen, Nano letters **12**, 2803 (2012).
 - [15] S. M. Young, F. Zheng, and A. M. Rappe, Physical review letters **109**, 236601 (2012).
 - [16] S. M. Young and A. M. Rappe, Physical review letters **109**, 116601 (2012).
 - [17] Z. Dai, A. M. Schankler, L. Gao, L. Z. Tan, and A. M. Rappe, Physical Review Letters **126**, 177403 (2021).
 - [18] Z. Dai and A. M. Rappe, Phys. Rev. B **104**, 235203 (2021).
 - [19] G. Dalba, Y. Soldo, F. Rocca, V. Fridkin, and P. Sainctavit, Physical review letters **74**, 988 (1995).
 - [20] Z. Chen, M. Segev, D. W. Wilson, R. E. Muller, and P. D. Maker, Physical Review Letters **78**, 2948 (1997).
 - [21] W. Ji, K. Yao, and Y. C. Liang, Advanced Materials **22**, 1763 (2010).
 - [22] C. Somma, K. Reimann, C. Flytzanis, T. Elsaesser, and M. Woerner, Physical review letters **112**, 146602 (2014).
 - [23] A. Zenkevich, Y. Matveyev, K. Maksimova, R. Gaynutdinov, A. Tolstikhina, and V. Fridkin, Physical Review B **90**, 161409 (2014).
 - [24] L. You, F. Zheng, L. Fang, Y. Zhou, L. Z. Tan, Z. Zhang, G. Ma, D. Schmidt, A. Rusydi, L. Wang, *et al.*, Science advances **4**, eaat3438 (2018).
 - [25] R. Fei, L. Z. Tan, and A. M. Rappe, Physical Review B **101**, 045104 (2020).
 - [26] M. Nakamura, S. Horiuchi, F. Kagawa, N. Ogawa, T. Kurumaji, Y. Tokura, and M. Kawasaki, Nature communications **8**, 1 (2017).
 - [27] M. Nakamura, H. Hatada, Y. Kaneko, N. Ogawa, Y. Tokura, and M. Kawasaki, Applied Physics Letters **113**, 232901 (2018).
 - [28] A. M. Burger, R. Agarwal, A. Aprelev, E. Schrub, A. Gutierrez-Perez, V. M. Fridkin, and J. E. Spanier,

- Science advances **5**, eaau5588 (2019).
- [29] A. M. Burger, L. Gao, R. Agarwal, A. Aprelev, J. E. Spanier, A. M. Rappe, and V. M. Fridkin, *Physical Review B* **102**, 081113 (2020).
 - [30] M.-M. Yang, D. J. Kim, and M. Alexe, *Science* **360**, 904 (2018).
 - [31] S. Nadupalli, J. Kreisel, and T. Granzow, *Science Advances* **5** (2019).
 - [32] Z. Gu, D. Imbrenda, A. L. Bennett-Jackson, M. Falmbigl, A. Podpirka, T. C. Parker, D. Shreiber, M. P. Ivill, V. M. Fridkin, and J. E. Spanier, *Physical review letters* **118**, 096601 (2017).
 - [33] L. Wu, A. Podpirka, J. E. Spanier, and P. K. Davies, *Chemistry of Materials* **31**, 4184 (2019).
 - [34] L. Wu, A. M. Burger, A. L. Bennett-Jackson, J. E. Spanier, and P. K. Davies, *Advanced Electronic Materials* **7**, 2100144 (2021).
 - [35] I. Grinberg, D. V. West, M. Torres, G. Gou, D. M. Stein, L. Wu, G. Chen, E. M. Gallo, A. R. Akbashev, P. K. Davies, *et al.*, *Nature* **503**, 509 (2013).
 - [36] Y. Bai, P. Tofel, J. Palosaari, H. Jantunen, and J. Juuti, *Advanced Materials* **29**, 1 (2017).
 - [37] O. Shafir, Y. Bai, J. Juuti, and I. Grinberg, *Phys. Rev. Applied* **14**, 044052 (2020).
 - [38] S. Das, S. Ghara, P. Mahadevan, S. Athinarayanan, J. Gopalakrishnan, and D. D. Sarma, *ACS Energy Letters* (2018).
 - [39] Z. Chen, C. Yuan, X. Liu, L. Meng, S. Cheng, J. Xu, C. Zhou, J. Wang, and G. Rao, *Materials Science in Semiconductor Processing* **115**, 105089 (2020).
 - [40] M. Zhong, C. Yuan, X. Liu, B. Zhu, L. Meng, C. Zhou, F. Liu, J. Xu, J. Wang, and G. Rao, *Materials Letters* **287**, 129299 (2021).
 - [41] Y. Zhang, T. Ideue, M. Onga, F. Qin, R. Suzuki, A. Zak, R. Tenne, J. Smet, and Y. Iwasa, *Nature* **570**, 349 (2019).
 - [42] J. Jiang, Z. Chen, Y. Hu, Y. Xiang, L. Zhang, Y. Wang, G.-C. Wang, and J. Shi, *Nature Nanotechnology* , 1 (2021).
 - [43] We note that due to the use of different illumination intensities in experiments, R_{SC} values rather than J_{SC} values should be used when comparing the BPE photocurrents obtained in different systems.
 - [44] S. Astafiev, V. Fridkin, and V. Lazarev, *Ferroelectrics* **80**, 251 (1988).
 - [45] C. Kittel, P. McEuen, and P. McEuen, *Introduction to solid state physics*, Vol. 8 (Wiley New York, 1996).
 - [46] T. Choi, S. Lee, Y. J. Choi, V. Kiryukhin, and S. W. Cheong, *Science* **324**, 63 (2009).
 - [47] G. Zhang, H. Wu, G. Li, Q. Huang, C. Yang, F. Huang, F. Liao, and J. Lin, *Scientific Reports* **3**, 10.1038/srep01265 (2013).
 - [48] H. Matsuo, Y. Noguchi, and M. Miyayama, *Nature Communications* **8**, 10.1038/s41467-017-00245-9 (2017).
 - [49] P. Lopez-Varo, L. Bertoluzzi, J. Bisquert, M. Alexe, M. Coll, J. Huang, J. Jimenez-Tejada, T. Kirchartz, R. Nechache, F. Rosei, and Y. Yuan, *Physics Reports* **563**, 1 (2016).
 - [50] F. Wang, S. M. Young, F. Zheng, I. Grinberg, and A. M. Rappe, *Nature communications* **7**, 1 (2016).
 - [51] A. H. Hubmann, S. Li, S. Zhukov, H. Von Seggern, and A. Klein, *Journal of Physics D: Applied Physics* **49**, 295304 (2016).
 - [52] M. Wittels and F. Sherrill, *Journal of Applied Physics* **28**, 606 (1957).
 - [53] P. Giannozzi, S. Baroni, N. Bonini, M. Calandra, R. Car, C. Cavazzoni, D. Ceresoli, G. L. Chiarotti, M. Cococcioni, I. Dabo, A. D. Corso, S. de Gironcoli, S. Fabris, G. Fratesi, R. Gebauer, U. Gerstmann, C. Gougoussis, A. Kokalj, M. Lazzeri, L. Martin-Samos, N. Marzari, F. Mauri, R. Mazzarello, S. Paolini, A. Pasquarello, L. Paulatto, C. Sbraccia, S. Scandolo, G. Sclauzero, A. P. Seitsonen, A. Smogunov, P. Umari, and R. M. Wentzcovitch, *Journal of Physics: Condensed Matter* **21**, 395502 (2009).
 - [54] J. P. Perdew, K. Burke, and M. Ernzerhof, *Phys. Rev. Lett.* **77**, 3865 (1996).
 - [55] X. Gonze, B. Amadon, G. Antonius, F. Arnardi, L. Baguet, J.-M. Beuken, J. Bieder, F. Bottin, J. Bouchet, E. Bousquet, N. Brouwer, F. Bruneval, G. Brunin, T. Cavignac, J.-B. Charraud, W. Chen, M. Côté, S. Cottenier, J. Denier, G. Geneste, P. Ghosez, M. Giantomassi, Y. Gillet, O. Gingras, D. R. Hamann, G. Hautier, X. He, N. Helbig, N. Holzwarth, Y. Jia, F. Jollet, W. Lafargue-Dit-Hauret, K. Lejaeghere, M. A. L. Marques, A. Martin, C. Martins, H. P. C. Miranda, F. Naccarato, K. Persson, G. Petretto, V. Planes, Y. Pouillon, S. Prokhorenko, F. Ricci, G.-M. Rignanese, A. H. Romero, M. M. Schmitt, M. Torrent, M. J. van Setten, B. V. Troeye, M. J. Verstraete, G. Zérah, and J. W. Zwanziger, *Comput. Phys. Commun.* **248**, 107042 (2020).
 - [56] M. van Setten, M. Giantomassi, E. Bousquet, M. Verstraete, D. Hamann, X. Gonze, and G.-M. Rignanese, *Computer Physics Communications* **226**, 39 (2018).
 - [57] P. Virtanen, R. Gommers, T. E. Oliphant, M. Haberland, T. Reddy, D. Cournapeau, E. Burovski, P. Peterson, W. Weckesser, J. Bright, S. J. van der Walt, M. Brett, J. Wilson, K. J. Millman, N. Mayorov, A. R. J. Nelson, E. Jones, R. Kern, E. Larson, C. J. Carey, Í. Polat, Y. Feng, E. W. Moore, J. VanderPlas, D. Laxalde, J. Perktold, R. Cimrman, I. Henriksen, E. A. Quintero, C. R. Harris, A. M. Archibald, A. H. Ribeiro, F. Pedregosa, P. van Mulbregt, and SciPy 1.0 Contributors, *Nature Methods* **17**, 261 (2020).
 - [58] O. Shafir, J. Yang, A. M. Rappe, and I. Grinberg, *Journal of Applied Physics* **126**, 174101 (2019).
 - [59] M. Stengel, P. Aguado-Puente, N. A. Spaldin, and J. Junquera., *Physical Review B* **83**, 235112 (2011).
 - [60] F. Chen and A. Klein, *Phys. Rev. B* **86**, 094105 (2012).
 - [61] N. Ramakrishnegowda, D. S. Knoche, L. Mühlenbein, A. Lotnyk, and A. Bhatnagar, *ACS Applied Nano Materials* **3**, 11881 (2020).
 - [62] G. Chen, K. Zou, Y. Yu, Y. Zhang, Q. Zhang, Y. Lu, and Y. He, *Ceramics International* **46**, 4148 (2020).
 - [63] H. Han, D. Kim, S. Chae, J. Park, S. Y. Nam, M. Choi, K. Yong, H. J. Kim, J. Son, and H. M. Jang, *Nanoscale* **10**, 13261 (2018).